

Lattice expansion, stability, and Mn solubility in substitutionally Mn-doped GaAs

Kohji Nakamura,* Keishi Hatano, Toru Akiyama, and Tomonori Ito
Department of Physics Engineering, Mie University, Tsu, Mie 514-8507, Japan

A. J. Freeman

Department of Physics and Astronomy, Northwestern University, Evanston, Illinois 60208, USA

(Received 3 November 2006; published 21 May 2007)

The structural properties and stability of zinc-blende $\text{Ga}_x\text{Mn}_{1-x}\text{As}$ over the whole Mn composition range are studied by means of the highly precise full-potential linearized augmented plane-wave method and the Connolly-Williams cluster expansion method, within the local-density approximation (LDA), generalized gradient approximation (GGA), and LDA+ U . In contrast to LDA and GGA predictions, the calculated LDA+ U lattice constant is found to increase when the Mn composition increases, even in the case that the Mn atoms substitutionally occupy cation sites, due to the correlation correction of the pd hybridization strength between the Mn $3d$ bands and the As $4p$ valence bands, which agrees with recent experimental findings. In addition, we confirm that the system has a tendency to segregate into GaAs and MnAs, and so inherently favors clustering. A temperature-composition phase diagram is obtained with the mean-field approximation for the entropy, in which the Mn solubility into GaAs is found to be very low at low temperatures (~ 300 °C).

DOI: [10.1103/PhysRevB.75.205205](https://doi.org/10.1103/PhysRevB.75.205205)

PACS number(s): 75.50.Pp, 71.15.Mb, 64.75.+g

I. INTRODUCTION

Understanding the structural properties and the stability of magnetic semiconductors may be of crucial importance in realizing novel spintronic applications. So far, many experimental and theoretical efforts¹⁻³ have been performed to clarify the structural, electronic, and magnetic properties of Mn-doped III-V semiconductors. The solubility of the Mn atoms has now been achieved up to about 10% by means of low-temperature molecular-beam epitaxy (MBE), which also increases the Curie temperature. Although the MBE growth introduces high Mn interstitial (Mn_i) and As antisite (As_{Ga}) defects, low-temperature annealing (200–300 °C) can eliminate most of the defects, and so the Mn atoms preferably occupy substitutional cation sites.^{4,5}

It is known experimentally that when Mn atoms are doped into GaAs, the lattice constant increases.¹ From first-principles studies based on the local-density approximation (LDA), the lattice expansion is explained due to the presence of the Mn_i and As_{Ga} defects, while the substitutional Mn atoms on the cation sites lead to a reduction in the lattice constant.^{6,7} However, recent experiments⁸ suggest that, even in the substitutional Mn case, the lattice constant is larger than that of GaAs, which is in contradiction to the LDA predictions. Although the LDA calculations have proven very successful in predicting electronic and magnetic structures in this material,⁹ there still remains a quantitative controversy; the photoemission experiments reveal a main Mn $3d$ peak at -4.4 eV relative to the Fermi level (E_F),^{10,11} but the LDA predicts it at -2 to -3 eV and overestimates the pd hybridization strength between the Mn $3d$ bands and the As $4p$ valence bands.^{12,13} This discrepancy is related to the fact that the LDA fails to describe the localized nature of the Mn $3d$ states. Indeed, recent LDA+ U calculations¹²⁻¹⁶ that incorporate additional on-site Coulomb correlation result in a better agreement with the photoemission spectra, in that the correlation effect pushes the Mn $3d$ majority-spin

(minority-spin) bands down (up) in energy and reduces the overestimated pd hybridization strength of the LDA. This reflects the importance of the strong Mn $3d$ correlation.

Since the structural properties and stability appear to be strongly governed by the electronic structures, one now needs a quantitative structural determination including the correlation effect such as the LDA+ U . Here, we investigate the structural properties and stability in zinc-blende $\text{Ga}_x\text{Mn}_{1-x}\text{As}$ over the whole Mn composition range by means of the highly precise full-potential linearized augmented plane-wave (FLAPW) method^{17,18} and the Connolly-Williams cluster expansion (CE) method,¹⁹ within the LDA,²⁰ generalized gradient approximation (GGA),²¹ and LDA+ U .²² In contrast to LDA and GGA predictions, we find that the calculated LDA+ U lattice constant increases when the substitutional Mn composition increases, which agrees with the recent experiments.⁸ In addition, we confirm that the system has a tendency to segregate into GaAs and MnAs, and so to inherently favor clustering. With the mean-field approximation for the entropy, we obtain a temperature-composition phase diagram, in which the Mn solubility into GaAs is found to be very low at low temperatures (~ 300 °C).

II. CALCULATIONS AND RESULTS

We first consider five ordered states having the zinc-blende structure: two constituent GaAs and MnAs, $\text{Ga}_{0.75}\text{Mn}_{0.25}\text{As}$ and $\text{Ga}_{0.25}\text{Mn}_{0.75}\text{As}$ with $L1_2$ structure, and $\text{Ga}_{0.5}\text{Mn}_{0.5}\text{As}$ with $L1_0$ structure with no tetragonal distortion, in which the Mn atoms substitutionally occupy cation sites. Local atomic relaxations of anions (As) that surround the Ga or Mn atoms are introduced in accordance with atomic force and total-energy calculations. Assuming ferromagnetic states, total energies E_n as a function of volume (V) for the ordered zinc-blende $\text{Ga}_{1-n/4}\text{Mn}_{n/4}\text{As}$ are calculated using the FLAPW method within the LDA, GGA, and

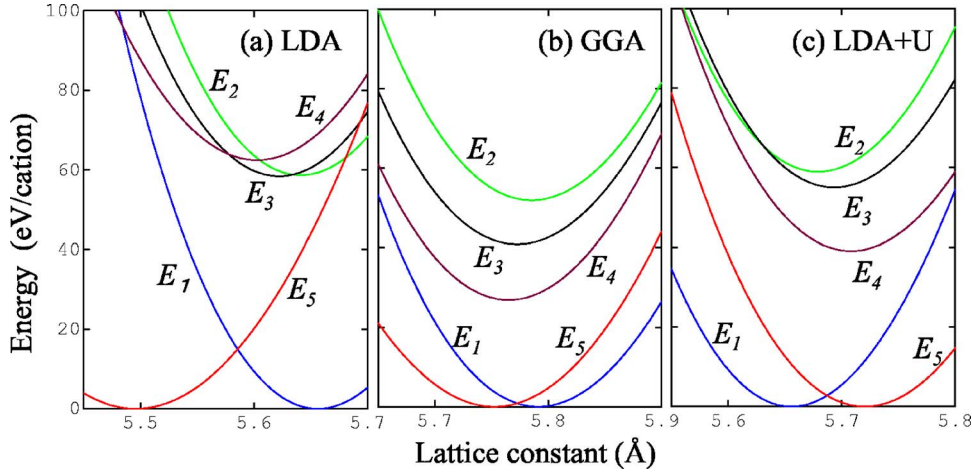


FIG. 1. (Color online) Calculated formation energy ΔE_n for five ordered zinc-blende $\text{Ga}_{1-n/4}\text{Mn}_{n/4}\text{As}$ as a function of lattice constant in the LDA, GGA, and LDA+ U .

LDA+ U , in which the core states are treated fully relativistically and the valence states are treated semirelativistically, i.e., without spin-orbit coupling. The Coulomb (U) and exchange (J) parameters used in the LDA+ U treatment for the Mn 3d states are the literature values of 4 and 0.7 eV, respectively.^{13,14} The LAPW basis with a cut off of $|\mathbf{k}+\mathbf{G}| \leq 3.9$ a.u.⁻¹ and muffin-tin sphere radii of 2.3 a.u. for the Ga and Mn and 2.0 a.u. for the As are used. Lattice harmonics with angular momentum up to $\ell=8$ are employed to expand the charge density, potential, and wave functions.

Then, we obtain the formation energy for the five ordered states, shown in Fig. 1, referred to the segregation limit as $\Delta E_n(V) = E_n(V) - [(1-x)E_{\text{GaAs}} + xE_{\text{MnAs}}]$, where $E_{\text{GaAs(MnAs)}}$ is the total energy of the constituent GaAs (MnAs), and the ΔE_n is fitted by the Murnaghan equation of state.²³ The results for the ordered states at their equilibrium volumes that minimize the ΔE_n with respect to the V are summarized in Table I.

Next, we estimate the formation energy for a disordered state (random solid solution), $\Delta E_D(V)$, by following the CE method,¹⁹ which was found to be successful for transition-metal binary alloys^{19,24} and III-V (and II-VI) semiconductor pseudobinary alloys.^{25,26} In general, the formation energy of a binary alloy with the specific atomic configuration n may be expressed with multisite correlation functions $\xi_{i,n}$ associated with i -point clusters as $\Delta E_n(V) = \sum_i v_i(V) \xi_{i,n}$, where $v_i(V)$ is an effective interatomic interaction of the i -point cluster as

a function of volume. With the $\Delta E_n(V)$ and *a priori* known $\xi_{i,n}$ ¹⁹ for the five ordered states, the $v_i(V)$ up to a tetrahedron cluster ($i=4$) can be extracted. We confirmed that the magnitude of the $v_i(V)$ turns out to be small when the cluster size becomes larger, and the $v_4(V)$ is much smaller than the others, as shown in Fig. 2, which fulfills an appropriate condition of the CE method.

Furthermore, in order to confirm the ability of the CE method, we estimate the formation energy and lattice constant via the CE method for a structure of zinc-blende $\text{Ga}_{0.875}\text{Mn}_{0.125}\text{As}$ (Fig. 3) that is not used in the CE method, and then compared them with directly calculated values by the FLAPW method including the local atomic relaxations of the As anions. The results at the equilibrium volume are given in Table II. The estimated values from the CE method agree very well with the directly calculated FLAPW values, differing by only 4 meV/cation in energy and by less than 0.01 Å in lattice constant, for all approximations. Of course, to obtain more quantitative results, an improved CE method²⁷ would be necessary.

With the $v_i(V)$ values obtained, the formation energy of the disordered state, in which the $\xi_{i,D}$ are given by $\xi_{i,D} = (1-2x)^i$ for the perfectly random atomic alignment, is calculated as $\Delta E_D(V) = \sum_i v_i(V) (1-2x)^i$. The results for the disordered state at the equilibrium volume that minimizes ΔE_D with respect to V are shown in Figs. 4 and 5.

TABLE I. Calculated formation energy ΔE_n^{min} at the equilibrium volumes referred to the segregation limit, lattice constant a , and interatomic distances to nearest neighbors of Ga-As ($d_{\text{Ga-As}}$) and Mn-As ($d_{\text{Mn-As}}$) for five ordered zinc-blende $\text{Ga}_{1-n/4}\text{Mn}_{n/4}\text{As}$ structures in the LDA, GGA, and LDA+ U .

| n | structure | ΔE (meV/cation) | | | a (Å) | | | $d_{\text{Ga-As}}$ (Å) | | | $d_{\text{Mn-As}}$ (Å) | | |
|-----|-----------|-------------------------|-----|----------|---------|-------|----------|------------------------|-------|----------|------------------------|-------|----------|
| | | LDA | GGA | LDA+ U | LDA | GGA | LDA+ U | LDA | GGA | LDA+ U | LDA | GGA | LDA+ U |
| 0 | fcc | 0 | 0 | 0 | 5.656 | 5.791 | 5.656 | 2.449 | 2.508 | 2.449 | | | |
| 1 | $L1_2$ | 59 | 52 | 59 | 5.641 | 5.785 | 5.679 | 2.451 | 2.518 | 2.458 | 2.419 | 2.465 | 2.463 |
| 2 | $L1_0$ | 59 | 41 | 55 | 5.622 | 5.773 | 5.693 | 2.450 | 2.514 | 2.445 | 2.419 | 2.485 | 2.486 |
| 3 | $L1_2$ | 63 | 27 | 30 | 5.604 | 5.765 | 5.708 | 2.455 | 2.512 | 2.455 | 2.417 | 2.491 | 2.477 |
| 4 | fcc | 0 | 0 | 0 | 5.496 | 5.753 | 5.720 | | | | 2.380 | 2.491 | 2.477 |

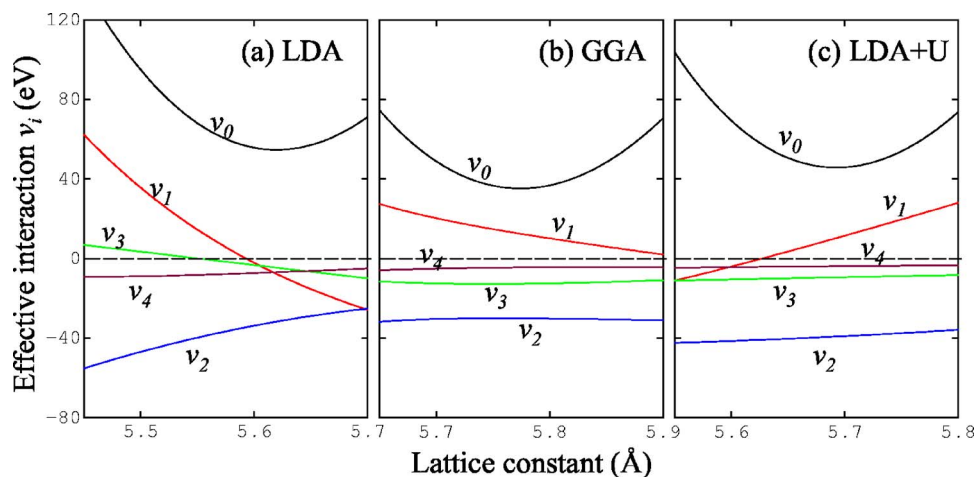


FIG. 2. (Color online) Calculated effective interaction energies, v_i ($i=0, 1, 2, 3$, and 4) as a function of lattice constant extracted by the cluster expansion method within the LDA, GGA, and LDA+ U .

III. DISCUSSION

A. Structural properties

As seen in Table I and Fig. 4, the calculated lattice constant is found to depend strongly on the approximation used. In the LDA and GGA, with increasing Mn composition, the lattice constant decreases compared to that of GaAs, which is inconsistent with the recent experiments⁸ mentioned above. Moreover, the calculated lattice constant of GaAs in the GGA, 5.791 Å, is much larger than the experimental value, 5.65 Å, although that in the LDA agrees well with the experimental value. For MnAs, the LDA calculated lattice constant, 5.496 Å, is much smaller than the experimental value, 5.69–5.73 Å, observed in the zinc-blende MnAs dots grown on the GaAs substrate,^{28–30,33} while the GGA gives a better prediction, as demonstrated previously.^{34–36} Although the experiments may measure the zinc-blende MnAs by the constrained substrate, the lattice constant in an unstrained zinc-blende MnAs is expected to be larger than that of the GaAs since the experimentally observed lattice constant of the MnAs dots is larger than that of the GaAs substrate. Thus, the commonly used LDA and GGA clearly fail in predicting the structural properties over the whole Mn composition range.

In contrast, the LDA+ U reproduces the experimental trends, namely, the lattice constant increases when the Mn

composition increases and that of MnAs, 5.720 Å, is almost consistent with the experimental values of the zinc-blende MnAs dots. The predicted lattice constants in the dilute region are parametrized as $a(x)=a_{\text{GaAs}}+0.09x$, although a small positive deviation from Vegard's law appears. Quantitatively, however, the theoretical prediction underestimates compared with the experimental one, $a(x)=a_{\text{GaAs}}+(0.26\pm 0.08)x$.⁸ This discrepancy may still be attributed to the theoretical approximation in the LDA+ U treatment and/or the effect of the As_{Ga} defects,⁷ which are stable up to ~ 450 °C,³¹ not being removed by the annealing in experiments.

The thermal effects on the structural properties, such as the lattice expansion due to changes of the atomic alignment (long-range and short-range orders) and the lattice vibration, may be important. In the former case, however, as seen in Fig. 4, almost no difference in the lattice constants between the ordered and random disordered states indicates that the effect of atomic alignment does not alter the structural properties. Also, since the thermal vibration expansion will be very small, as expected from the III-V semiconductors,³² compared to the lattice constant of GaAs and MnAs, this effect again may not significantly change the structural properties.

Table I gives calculated interatomic distances to the nearest neighbors, i.e., the Ga and As atoms (Ga-As) and the Mn and As atoms (Mn-As), in which both Mn-As and Ga-As distances do not change over the whole Mn composition. In the LDA and GGA, the Mn-As distance is always smaller than the Ga-As distance, indicating that the bonding of the Mn-As is stronger than that in the Ga-As, so as to contract the lattice when the Mn composition increases. In the LDA

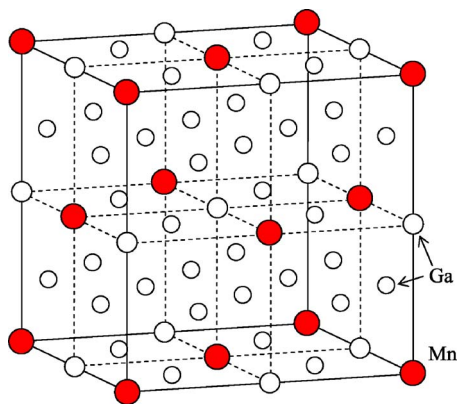


FIG. 3. (Color online) Structure of zinc-blende $\text{Ga}_{0.875}\text{Mn}_{0.125}\text{As}$, where Ga and Mn atoms are represented by open and closed circles, respectively, and As atoms are not given.

TABLE II. Comparison of formation energies and lattice constants calculated by the CE method and by FLAPW method for zinc-blende $\text{Ga}_{0.875}\text{Mn}_{0.125}\text{As}$ in the LDA, GGA, and LDA+ U .

| | ΔE (meV/cation) | | | a (Å) | | |
|-------|-------------------------|-----|----------|---------|-------|----------|
| | LDA | GGA | LDA+ U | LDA | GGA | LDA+ U |
| CE | 30 | 26 | 30 | 5.648 | 5.787 | 5.667 |
| FLAPW | 27 | 23 | 26 | 5.649 | 5.788 | 5.667 |

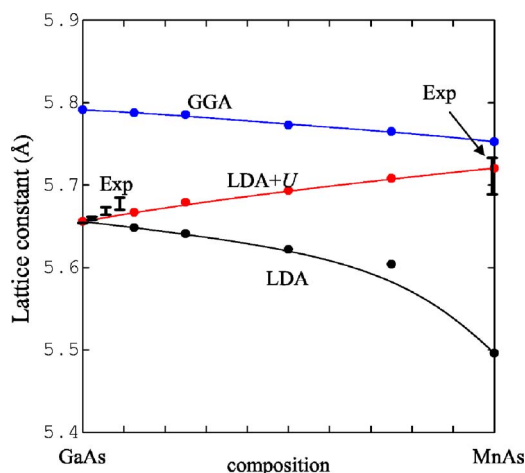


FIG. 4. (Color online) Calculated lattice constant for the ordered (circles) and random disordered (lines) states of zinc-blende $\text{Ga}_{1-x}\text{Mn}_x\text{As}$ as a function of Mn composition (x) in the LDA, GGA, and LDA+ U . Bars indicate experimental results for diluted Mn-doped zinc-blende GaAs solid solutions (Ref. 8) and zinc-blende MnAs dots grown on a GaAs substrate (Refs. 28–30 and 33).

+ U , however, the Mn-As distance turns out to be larger than the Ga-As one due to the correlation correction of the pd hybridization strength,^{12,13} which leads to the lattice expansion as seen in Fig. 4.

In order to understand the effect of correlation on the structural properties, we performed LDA and LDA+ U calculations for $\text{Ga}_{0.75}\text{Mn}_{0.25}\text{As}$ with the $L1_2$ structure assuming the same lattice constant (5.65 Å) with the ideal As positions ($d_{\text{Mn-As}}=d_{\text{Ga-As}}$). Figure 6 shows the density of states in the LDA and LDA+ U and the difference in charge density ($\Delta\rho$) between the LDA and LDA+ U on the (110) plane. In the LDA, the Mn $3d t_g$ majority-spin bands strongly hybridize

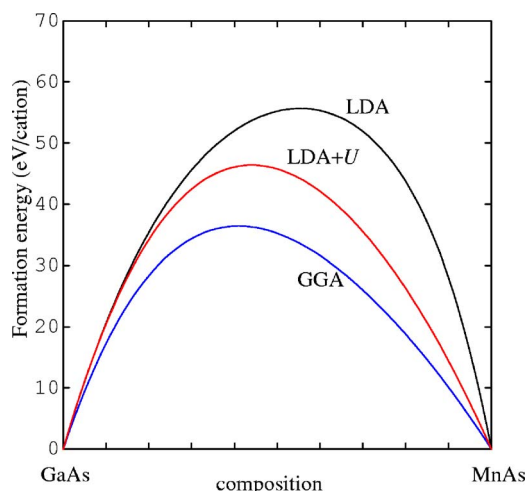


FIG. 5. (Color online) Calculated formation energy for the random disordered state of zinc-blende $\text{Ga}_{1-x}\text{Mn}_x\text{As}$ as a function of Mn composition (x) in the LDA, GGA, and LDA+ U .

with As $4p$ bands with the bonding and antibonding states, where the Fermi level (E_F) is located in the antibonding state. As pointed out previously,^{12,13} however, the correlation effect greatly localizes the Mn $3d$ states and pushes the majority-spin states down in energy so as to move them to the bottom of the valence state. Thus, the pd hybridization is reduced by the correlation, compared to the LDA case, and the majority-spin $3d$ state (antibonding state) is much more occupied. The $\Delta\rho$ in Fig. 6(c) clearly shows charge accumulation/depletion with an antibonding character in the Mn-As neighbor but no change in the Ga-As neighbor, which may cause an increase of the Mn-As distance but no change in the Ga-As distance.

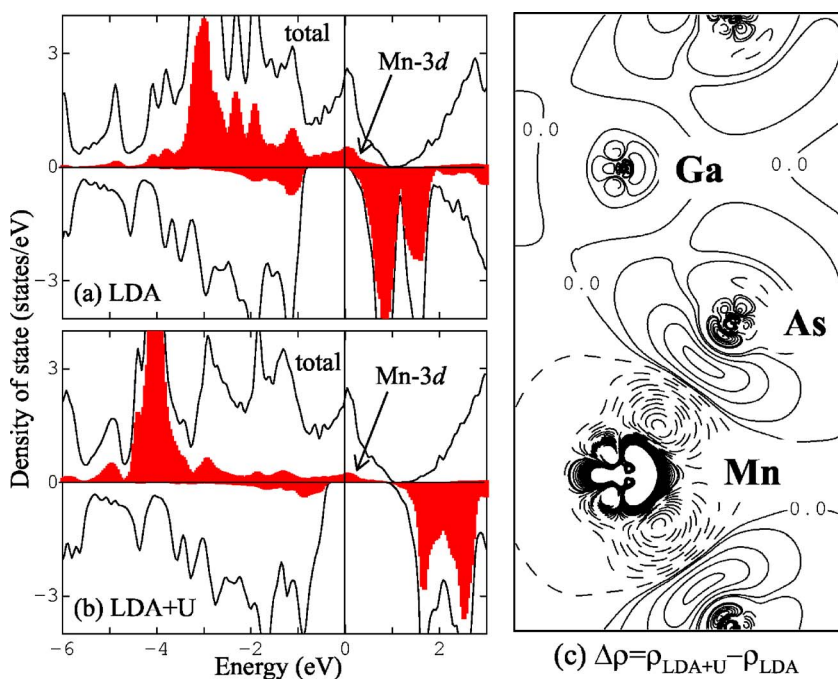


FIG. 6. (Color online) Calculated total and partial Mn $3d$ densities of states (DOS) in the LDA and LDA+ U , and difference in charge density ($\Delta\rho$) between the LDA and LDA+ U on the (110) plane, where the solid and dash lines represent positive and negative values of the charge difference, respectively, and adjacent contours differ by 3×10^{-4} electrons/a.u.³. Calculations are performed for $\text{Ga}_{0.75}\text{Mn}_{0.25}\text{As}$ with the $L1_2$ structure assuming a lattice constant of 5.65 Å with an ideal As atom position.

B. Phase stability

The calculated formation energies of the ordered and disordered states in all approximations, as seen in Table I and Fig. 5, have positive values; these phases are less favorable with respect to a phase separation, and so this system has a tendency to segregate. However, some differences among these approximations appear; an asymmetry in the formation energy with respect to the Mn composition in the LDA differs from those in the GGA and LDA+ U , and the magnitude in the LDA is larger than that in the LDA+ U while that in the GGA is smaller. Note that the trend in the formation energy in the LDA+ U and GGA results in Fig. 5 is close to the results that were recently predicted from first-principles GGA calculations combined by the mixed-basis CE method.²⁷

In understanding the phase stability, the lattice mismatch between the constituent GaAs and MnAs, $\Delta r/\bar{r}$ (where Δr and \bar{r} are the difference and average of both lattice constants) is one of the most important properties, as discussed for the III-V semiconductor pseudobinary alloys.²⁶ In the present Ga_{1-x}Mn_xAs case, $\Delta r/\bar{r}$ in the LDA+ U (also in the GGA) results in a small value of 1%, which therefore plays a minor role in determining the phase stability. In contrast, the lattice mismatch in the LDA, 3%, is not negligibly small, and the elastic energy contribution attributed to this lattice mismatch may enhance the positive formation energy of the disordered state, as seen in Fig. 5.

Finally, we calculate a temperature-composition phase diagram of the zinc-blende Ga_{1-x}Mn_xAs alloy based on the LDA+ U . In the disordered state with random atomic alignment, the free energy is given as $F(x)=\Delta E_D(x)-k_B T S_D(x)$, where $\Delta E_D(x)$ and $S_D(x)$ are the formation energy (Fig. 5) and the entropy of mixing, respectively, of the random disordered state. Here, the $\Delta E_D(x)$ is fitted by a linear equation, $\Delta E_D(x)=\sum_i \Omega_i x^{i-1}$, and the $S_D(x)$ is described by the mean-field approximation, $-k_B[x \ln x+(1-x) \ln(1-x)]$. Then, we obtain the binodal and spinodal lines by numerically calculating conditions for the common tangent³⁷ and $d^2F(x)/dx^2=0$, respectively.

The results, as presented in Fig. 7, show a phase-separated-type phase diagram with a miscibility gap with a critical temperature of about 1130 K, in which the thermodynamic equilibrium Mn solubility into GaAs is very low at low temperatures, namely, 1 at. % at 300 °C. The spinodal decomposition occurs for more than about 0.1 Mn composition at the low temperatures, which leads to a phase instability of the single solid solution against the phase separation. This may give a Mn solubility limit in the nonequilibrium condition. The experimental solubility, such as obtained by the low-temperature MBE,¹ has almost been achieved in our predicted solubility limit. Of course, the spinodal decomposition now opens a way to control nanoscale network structures.³⁸

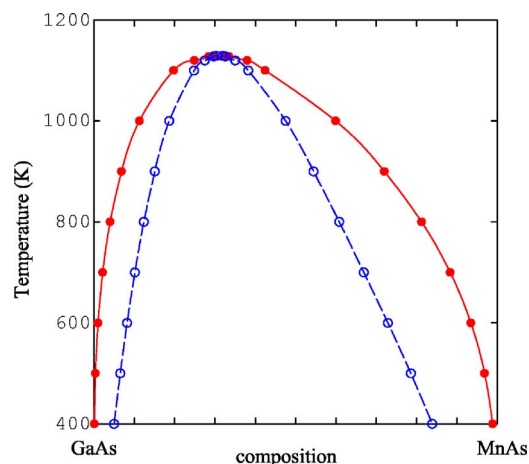


FIG. 7. (Color online) Calculated temperature-composition phase diagram for zinc-blende Ga_{1-x}Mn_xAs based on LDA+ U , which is obtained with the mean-field approximation. Solid and dashed lines correspond to binodal and spinodal lines, respectively.

IV. SUMMARY

We investigated the structural properties and stability in zinc-blende Ga_xMn_{1-x}As over the whole Mn composition by means of the FLAPW method and the CE method, within the LDA, GGA, and LDA+ U . The LDA and GGA predict that the substitutional Mn atoms on the cation sites lead to a reduction in the lattice constant, while in the LDA+ U , the lattice constant increases when the Mn composition increases due to the correlation correction of the pd hybridization strength; the latter agrees with the recent experimental results. We also confirm that the system has the tendency to segregate into GaAs and MnAs, and so inherently favors clustering. Using the mean-field approximation for the entropy, we demonstrated the phase-separated-type phase diagram with the miscibility gap with a critical temperature of about 1130 K and determined the spinodal decomposition region.

ACKNOWLEDGMENTS

Work at Mie University was supported by a Grant-in-Aid for Scientific Research from the Ministry of Education, Science, Sport, and Culture of Japan and performed for computations at the Cooperative Research Center and Center for Information Technologies and Networks, Mie University, and the Supercomputer Center, Institute for Solid State Physics, University of Tokyo. Work at Northwestern University was supported by the U.S. National Science Foundation (through its MRSEC program at the NU Materials Research Center).

*Email address: kohji@phen.mie-u.ac.jp

- ¹H. Ohno, J. Magn. Magn. Mater. **200**, 110 (1999).
- ²A. H. MacDonald, P. Schiffer, and N. Samarth, Nat. Mater. **4**, 195 (2005).
- ³T. Jungwirth, J. Sinova, J. Mašek, J. Kučera, and A. H. MacDonald, Rev. Mod. Phys. **78**, 809 (2006).
- ⁴S. J. Potashnik, K. C. Ku, S. H. Chun, J. J. Berry, N. Samarth, and P. Schiffer, Appl. Phys. Lett. **79**, 1495 (2001).
- ⁵K. M. Yu, W. Walukiewicz, T. Wojtowicz, I. Kuryliszyn, X. Liu, Y. Sasaki, and J. K. Furdyna, Phys. Rev. B **65**, 201303(R) (2002).
- ⁶J. Mašek, J. Kudrnovsky, and F. Maca, Phys. Rev. B **67**, 153203 (2003).
- ⁷J. Mašek and F. Maca, Acta Phys. Pol. A **108**, 789 (2002).
- ⁸L. X. Zhao, C. R. Staddon, K. Y. Wang, K. W. Edmonds, R. P. Champion, B. L. Gallagher, and C. T. Foxon, Appl. Phys. Lett. **86**, 071902 (2005).
- ⁹S. Sanvito, G. Theurich, and N. A. Hill, J. Supercond. **15**, 85 (2002).
- ¹⁰J. Okabayashi, A. Kimura, T. Mizokawa, A. Fujimori, T. Hayashi, and M. Tanaka, Phys. Rev. B **59**, R2486 (1999).
- ¹¹O. Rader, C. Pampuch, A. M. Shikin, W. Gudat, J. Okabayashi, T. Mizokawa, A. Fujimori, T. Hayashi, M. Tanaka, A. Tanaka, and A. Kimura, Phys. Rev. B **69**, 075202 (2004).
- ¹²L. M. Sandratskii, P. Bruno, and J. Kudrnovsky, Phys. Rev. B **69**, 195203 (2004).
- ¹³A. B. Shick, J. Kudrnovsky, and V. Drchal, Phys. Rev. B **69**, 125207 (2004).
- ¹⁴J. H. Park, S. K. Kwon, and B. I. Min, Physica B **281&282**, 703 (2000).
- ¹⁵B. Sanyal, O. Bengone, and S. Mirbt, Phys. Rev. B **68**, 205210 (2003).
- ¹⁶K. Sato, P. H. Dederichs, and H. Katayama-Yoshida, Physica B **376&377**, 639 (2006).
- ¹⁷E. Wimmer, H. Krakauer, M. Weinert, and A. J. Freeman, Phys. Rev. B **24**, 864 (1981).
- ¹⁸M. Weinert, E. Wimmer, and A. J. Freeman, Phys. Rev. B **26**, 4571 (1982).
- ¹⁹J. W. D. Connolly and A. R. Williams, Phys. Rev. B **27**, 5169(R) (1983).
- ²⁰U. von Barth and L. Hedin, J. Phys. C **5**, 1629 (1972).
- ²¹J. P. Perdew, K. Burke, and M. Ernzerhof, Phys. Rev. Lett. **77**, 3865 (1996).
- ²²A. B. Shick, A. I. Liechtenstein, and W. E. Pickett, Phys. Rev. B **60**, 10763 (1999).
- ²³F. D. Murnaghan, Proc. Natl. Acad. Sci. U.S.A. **30**, 244 (1944).
- ²⁴K. Terakura, T. Oguchi, T. Mohri, and K. Watanabe, Phys. Rev. B **35**, 2169 (1987).
- ²⁵S. H. Wei, L. G. Ferreira, and A. Zunger, Phys. Rev. B **41**, 8240 (1990).
- ²⁶T. Mohri, K. Nakamura, and T. Ito, J. Appl. Phys. **70**, 1320 (1991).
- ²⁷J. Osorio-Guillén, Y. J. Zhao, S. V. Barabash, and A. Zunger, Phys. Rev. B **74**, 035305 (2006).
- ²⁸J. Okabayashi, M. Mizuguchi, K. Ono, M. Oshima, A. Fujimori, H. Kuramochi, and H. Akinaga, Phys. Rev. B **70**, 233305 (2004).
- ²⁹H. Ofuchi, J. Okabayashi, M. Mizuguchi, M. Yamada, K. Ono, Y. Takeda, M. Ohshima, and A. Akinaga, Phys. Scr., T **115**, 431 (2005).
- ³⁰H. C. Jeo, T. W. Kang, Sh. U. Yuldashev, T. W. Kim, and S. Jin, Appl. Phys. Lett. **89**, 112517 (2006).
- ³¹D. E. Bliss, W. Walukiewicz, J. W. Ager III, E. E. Haller, K. T. Chan, and S. Tanigawa, J. Appl. Phys. **71**, 1699 (1992).
- ³²T. Mohri and K. Nakamura, 11th Record of Alloy Semiconductor Physics and Electronics Symposium, 1992, p. 181.
- ³³T. W. Kim, H. C. Jeo, T. W. Kang, H. S. Lee, and S. Jin, Appl. Phys. Lett. **88**, 021915 (2006).
- ³⁴A. Continenza, S. Picozzi, W. T. Geng, and A. J. Freeman, Phys. Rev. B **64**, 085204 (2001).
- ³⁵Y. J. Zhao, W. T. Geng, A. J. Freeman, and B. Delley, Phys. Rev. B **65**, 113202 (2002).
- ³⁶Y. J. Zhao and A. Zunger, Phys. Rev. B **71**, 132403 (2005).
- ³⁷R. A. Swalin, *Thermodynamics of Solid* (Wiley, New York, 1962).
- ³⁸K. Sato, H. Katayama-Yoshida, and P. H. Dederichs, Jpn. J. Appl. Phys., Part 2 **30**, L948 (2005).